PROCEEDINGS OF ECOS 2026 – THE 39th INTERNATIONAL CONFERENCE ON

EFFICIENCY, COST, OPTIMIZATION, SIMULATION AND ENVIRONMENTAL IMPACT OF ENERGY SYSTEMS

28 JUNE – 03 JULY, 2026, CONSTANTA, ROMANIA

Network-Constrained Nonlinear Optimization Framework for Integrated Multi-Energy System Decarbonization

***Mattia Calabrese*[a], *Michele Francesconi*[b], *Carlo Carcasci*[c]**

[a] *Università degli Studi di Firenze, Department of Industrial Engineering (DIEF), Via di Santa Marta 3, 50139 Florence, Italy, mattia.calabrese@unifi.it, CA*

[b] *Università degli Studi di Firenze, Department of Industrial Engineering (DIEF), Via di Santa Marta 3, 50139 Florence, Italy, michele.francesconi@unifi.it*

[c] *Università degli Studi di Firenze, Department of Industrial Engineering (DIEF), Via di Santa Marta 3, 50139 Florence, Italy, carlo.carcasci@unifi.it*

Abstract:

The modeling of integrated energy systems is increasingly central to the assessment of decarbonization pathways in the context of rapid electrification, high renewable energy penetration, and growing sector coupling. Addressing these challenges requires optimization frameworks capable of representing interactions across multiple energy carriers while preserving physical and operational feasibility. In particular, both technological performance and infrastructure constraints introduce non-linear behaviors that are often simplified or neglected in system-level analyses. This work presents a multi-node, multi-energy vector system optimization model formulated as a non-linear programming (NLP) problem. Infrastructure transport limits are modeled through carrier-specific network constraints, capacity bounds, flow-dependent losses, and pressure or loading limits, ensuring physically consistent energy exchanges across the system. The framework is applied to a representative regional-scale energy system to explore alternative decarbonization pathways. System performance is evaluated using a Levelized Cost of Final Energy (LCFE) metric, providing an integrated techno-economic measure of whole-system costs across scenarios. Results show that renewable expansion alone can reduce emissions from 9.58 to 7.68 Mt_{CO_2} while decreasing system costs (LCFE from 53.0 to 46.9 €/MWh). However, deeper decarbonization through electrification and hydrogen integration requires substantial infrastructure investments, increasing system costs up to 80.3 €/MWh in high-electrification scenarios and 130.3 €/MWh in a fully decarbonized configuration. The latter also reveals significant transmission constraints, indicating the need for grid reinforcement. Overall, the analysis highlights a transition from fuel-driven to capital-intensive systems, where flexibility provided by storage and sector coupling becomes essential. The proposed framework enables realistic and physically grounded assessment of decarbonization pathways, supporting more robust planning of integrated multi-energy systems.

Keywords:

Energy Systems; Multi-energy Optimization; Hydrogen; Network Constraints; Decarbonization.

1. Introduction

Achieving climate neutrality by mid-century requires a profound transformation of regional energy systems, extending beyond the large-scale deployment of Renewable Energy Sources (RES) to a systemic reorganization of energy production, transport, conversion, and consumption. Scenario analyses with energy system and integrated assessment models consistently indicate that net-zero pathways rely on extensive electrification, rapid expansion of wind and solar generation, and the progressive integration of hydrogen as a complementary energy carrier [1].

At the regional scale, decarbonization pathways are shaped by local renewable availability, network topology, spatially distributed demand, and interactions among multiple energy carriers. Sector coupling, namely the coordinated integration of electricity, gas, hydrogen, and heat systems, has emerged as a cornerstone of deep decarbonization strategies [2]. Electrification often represents the most cost-effective abatement route, while hydrogen plays a targeted but essential role in hard-to-abate sectors such as industry and heavy transport.

The effectiveness of these strategies, however, depends critically on infrastructure capacity to accommodate new flows, storage patterns, and conversion processes.

Recent studies demonstrate that hydrogen infrastructure planning and cross-regional exchanges can significantly influence technology deployment and system costs. A unified European hydrogen backbone, for instance, reshapes production geography and reinforces inter-dependencies between renewable-rich and demand regions [3]. Similarly, analyses of power-to-gas-to-power systems show that hydrogen's flexibility value is highly sensitive to spatial resolution and network constraints [4]. Neglecting infrastructure bottlenecks and spatial coupling may therefore underestimate costs and overstate self-sufficiency.

Regional systems constitute a critical analytical scale. Unlike highly aggregated national models, regional studies can capture localized transmission constraints, congestion, and geographically differentiated technology deployment, while remaining suitable for strategic scenario analysis. At the same time, regions are embedded within broader energy networks: electricity and gas/hydrogen exchanges between nodes can fundamentally reshape dispatch, investments, and infrastructure utilization. Ignoring these interactions risks misrepresenting the operational feasibility of deep decarbonization, especially under high renewable penetration and accelerated electrification.

Despite growing recognition of these issues, many studies still adopt simplified spatial representations, modeling regions as single nodes or assuming unconstrained exchanges. While appropriate for high-level assessments, such abstractions may overlook binding network capacities, transport losses, and operational limits that become decisive in highly renewable systems. The literature increasingly identifies electrical and hydrogen transport infrastructures as potential bottlenecks influencing both system configuration and the relative competitiveness of alternative decarbonization options [5, 6].

The Italian region of Tuscany provides a representative and policy-relevant case study. Its diversified energy mix, significant renewable potential, and heterogeneous spatial distribution of generation and demand make it well-suited to investigate how progressively stringent emission targets reshape system operation when node-to-node exchanges are explicitly modeled.

Against this background, this work applies a multi-node, multi-energy optimization framework to assess alternative decarbonization pathways in a real regional system. Electricity and gas/hydrogen networks are explicitly represented to ensure physically consistent energy exchanges and transport. The analysis examines how increasingly ambitious emission targets modify generation portfolios, conversion technologies, energy flows, and infrastructure utilization. Scenarios are evaluated from an integrated techno-economic perspective using levelized cost of energy metrics, enabling consistent comparison across pathways while accounting for generation, storage, conversion, and transport. Particular attention is given to flexibility provision through storage and sector coupling.

This work provides a spatially resolved assessment of regional decarbonization pathways, quantifying the role of node-to-node exchanges and clarifying the structural conditions under which sector coupling and hydrogen deployment become necessary to achieve ambitious emission targets. Overall, the results underscore the importance of spatially explicit regional analyses for designing robust decarbonization strategies in highly renewable and electrified futures.

2. Materials and methods

2.1. Model Description

A multi-energy carrier optimization model was developed to simulate the operation of an integrated electricity, natural gas, and hydrogen system. The model is implemented in Python using IPOPT (Interior Point OPTimizer) in the Pyomo Environment and formulated as a Non-Linear Programming (NLP) optimization problem. The system is represented as a directed graph composed of nodes N and vector-specific edges E_v. Nodes represent geographical or functional aggregation points where production, demand, and energy conversion processes occur, while edges represent physical transport infrastructures, such as electric transmission lines and gas pipelines. Each energy vector is modeled at the flow level, while interactions between vectors are introduced through nodal coupling terms, such as gas turbines for gas-electricity networks and electrolyzer for hydrogen-electricity. The network topology is assumed fixed over the simulation horizon, and the problem is solved with hourly resolution. Storage dynamics are described through recursive state-of-charge equations, and compressor energy consumption is included whenever required by pressure differentials between connected nodes.

For each node n, energy vector v, and time step t, energy conservation is enforced through the nodal balance equation, represented in Eq. (1):

$$\sum_{i \in N} P^{in}_{i,n,t} \; + \; P^{dis}_{n,t} \; = \; \sum_{j \in N} P^{out}_{n,j,t} \; + \; P^{dem}_{n,t} \; + \; P^{curt}_{n,t} \tag{1}$$

where $P^{in}_{i,n,t}$ and $P^{out}_{n,j,t}$ denote inflows and outflows, $P^{dis}_{n,t}$ is the dispatch, $P^{dem}_{n,t}$ represents the demand, and $P^{curt}_{n,t}$ is the curtailed renewable energy at node n, included only for electricity balances.

The objective function aims at minimizing the total operating costs of the system over the considered time horizon and is given in Eq. (2):

$$\min \sum_{n \in N} C^{O\&M}_{n} \; + \sum_{v \in V} \sum_{t \in T} P^{grid}_{v,t} \cdot c_{v,t} \tag{2}$$

where $C^{O\&M}_{n}$ represents annual operation and maintenance costs, expressed as a fraction of investment costs, $P^{grid}_{v,t}$ is the imported energy of vector v at time t, and $c_{v,t}$ is the corresponding purchase price.

Furthermore, grid constraints are imposed on all energy vectors. The formulation differs between electricity lines and hydrogen and natural gas pipelines; however, in general, each node is associated with coordinates x_n and y_n. These allow the calculation of the Euclidean distance between nodes i and j.

Electricity flows are modeled using a linearized Direct Current (DC) power flow approximation [7]. This formulation is derived from the nonlinear Alternating Current (AC) power flow equations under the assumptions that all per-unit voltage magnitudes are close to unity; line resistance $r_{i,j}$ is negligible compared to line reactance $x_{i,j}$; voltage angle differences are small ($\sin(\theta_i - \theta_j) \approx (\theta_i - \theta_j)$ and $\cos(\theta_i - \theta_j) \approx 0$); reactive power flows are negligible compared to active power flows.

Under these assumptions, active power flow can be expressed as:

$$P^{el}_{i,j,t} = \frac{\theta_{i,t} - \theta_{j,t}}{x_{i,j}} \tag{3}$$

The voltage angles are bounded between a minimum and a maximum value, as expressed in Eq. (4):

$$\theta^{min}_{i} \; \leq \; \theta_{i,t} \; \leq \; \theta^{max}_{i} \tag{4}$$

One node is designated as the slack node, where the voltage angle is fixed. This reference condition provides the angular datum of the system and ensures a unique solution of the DC power flow equations.

With the same assumptions, power losses are approximated as in Eq. (5):

$$P^{el,loss}_{i,j,t} = r_{i,j} \cdot dist_{i,j} \cdot P^{el}_{i,j,t} \, |P^{el}_{i,j,t}| \tag{5}$$

where the absolute value ensures consistency with bidirectional flows.

A different formulation is presented for hydrogen and natural gas pipelines. In gaseous networks, transport losses are modeled through pressure drops along the pipelines rather than reductions in mass flow rate. For each node, pressure is bounded between a minimum and a maximum value:

$$p^{min}_{i} \; \leq \; p_{i,t} \; \leq \; p^{max}_{i} \tag{6}$$

The pressure drop along a pipeline is expressed as in Eq. (7):

$$p^2_{i,t} - p^2_{j,t} = \frac{8 \, f \, Z \, T \, R_{gas}}{\pi^2} \frac{dist_{i,j}}{D^5} \, \dot{m}_{i,j,t} \, |\dot{m}_{i,j,t}| \tag{7}$$

where D is the pipe diameter, $\dot{m}_{i,j,t}$ is the mass flow rate, f is the Darcy friction factor, Z is the compressibility factor, T is the temperature, and R_{gas} is the specific gas constant, which differs for hydrogen and natural gas [8].

Certain nodes are designated as injection nodes with fixed pressure values, establishing the hydraulic boundary conditions required to compute the consistent network pressure distribution.

For all energy vectors, transport capacity constraints are imposed:

$$-Cap^{v}_{i,j} \; \leq \; P^{v}_{i,j,t} \; \leq \; Cap^{v}_{i,j} \tag{8}$$

These constraints ensure compliance with infrastructure limits and prevent non-physical flows.

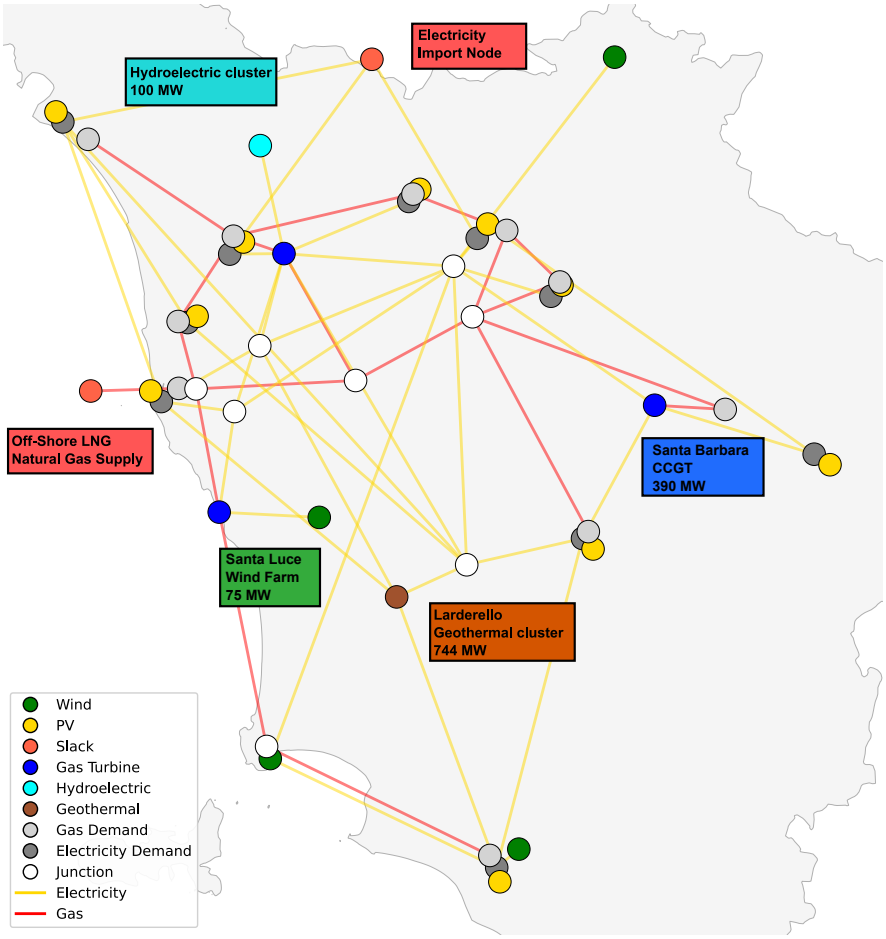

Figure 1. *Electric and gas network of Tuscany in the reference scenario. Circles represent electric buses and gas network nodes, connections represent electric power lines and gas network pipelines.*

In this study, the developed framework is applied to a real regional energy system, allowing the evaluation of spatial energy flows, infrastructure constraints, and cross-vector interactions under progressive decarbonization pathways.

2.2. Case Study and Scenario Definition

To demonstrate the applicability of the proposed optimization framework, the model was applied to the regional energy system of Tuscany (Italy). The case study provides a geographically consistent representation of the interaction between the high-voltage electricity transmission network and the high-pressure natural gas transmission system, covering all ten provinces of the region. The regional model is conceived as a physically coherent but synthetic reconstruction derived from publicly available datasets. The modeled network topology, including nodes and interconnections, is illustrated in Figure 1.

The baseline natural gas network reflects the regional backbone infrastructure and includes a primary supply node corresponding to the Offshore LNG Toscana terminal in Livorno. Pipeline diameters and admissible pressure limits were obtained from [9]. Minor interconnections with the national gas grid, located in boundary provinces, are not treated as independent supply nodes. Instead, their contribution is incorporated implicitly through an adjustment of nodal demand. At these boundary nodes, total provincial gas demand is partitioned between the modeled regional network and the external national system proportionally to the diameters of the connected pipelines. This approach preserves mass balance consistency while maintaining model tractability.

The electricity transmission system is simplified considering lines operating at 380 kV. The network was reconstructed using facility coordinates data from OpenInfraMap [10] and the RSE dataset [11]. Transmission limits were derived from the maximum admissible thermal currents specified by Italian technical standards [12]. A reference current limit of 2310 A was assumed, and the corresponding apparent power limits were calculated accordingly. The generation portfolio includes all operational plants above 20 MW as of 2024 [11]. The baseline renewable configuration reflects currently operational RES plants. For modeling purposes, selected facilities, such as the geothermal cluster, were aggregated, and provincial-level installed PV capacities were considered to reduce computational complexity while preserving total installed capacity and geographical distribution. Hourly renewable generation profiles were obtained from the PVGIS database [13], enabling spatially

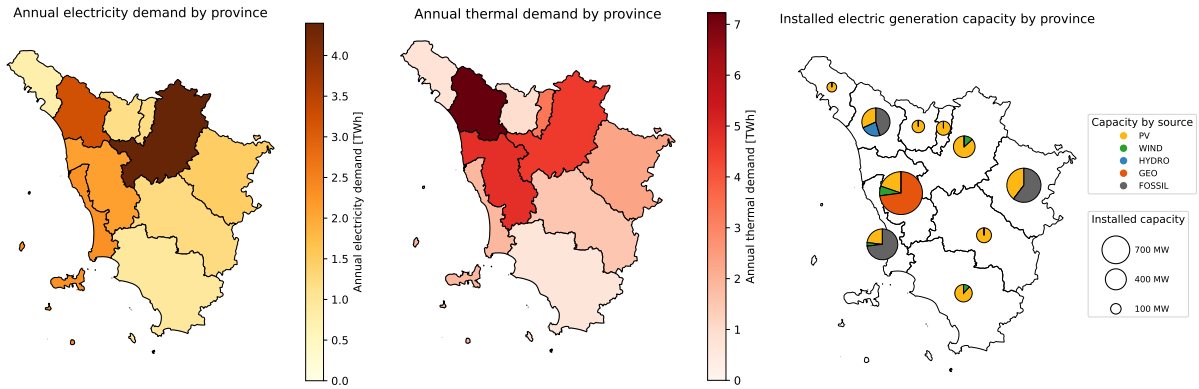

Figure 2. *Mean annual electric demand (left), thermal demand (center), and installed electric generation (right) across Tuscan provinces.*

differentiated representation of solar and wind resource availability across provinces.

Electricity and natural gas demand were reconstructed at provincial scale and translated into hourly time series consistent with the temporal resolution of the optimization model. For electricity, hourly demand profiles were generated using the RSE TOTEM software [11], ensuring realistic load variability. For natural gas, provincial annual demand data were sourced from [14]. Hourly sectoral profiles were derived from Guzzo et al. [8]. To account for stochastic variability, random perturbations were introduced: $\pm 2\%$ for industrial demand and $\pm 5\%$ for the residential sector. Seasonal variability in non-industrial consumption was incorporated through a tuning factor applied to heating-related loads. The tuning factor was set to 0.5 during intermediate seasons and 0.1 in summer. The spatial allocation of annual electricity and gas demand across provinces is illustrated in Figure 2, in conjunction with the installed power plant capacities, thereby emphasizing geographical heterogeneity in consumption and production patterns.

To evaluate the response of the integrated regional system under progressively stringent decarbonization pathways, five structurally distinct scenarios were defined. Each scenario modifies the boundary conditions of the optimization problem by altering generation capacities, demand composition, and energy vector interactions.

- **Scenario 1 – Reference System (REF)**

  The reference scenario reproduces the current configuration of the regional energy system, including existing generation capacities, infrastructure topology, and present electricity and natural gas demand levels. No additional renewable capacity, electrification measures, or hydrogen integration are introduced. This configuration represents the present-day operational state of the system and serves as the baseline against which all alternative decarbonization pathways are evaluated in terms of energy flows, system costs, and emissions.

- **Scenario 2 – Renewable Expansion (RES+)**

  In this scenario, renewable generation capacity is increased according to currently approved and planned projects [15]. This results in 1.82 GW of additional PV and 2.24 GW of additional wind, with a particular concentration in the province of Grosseto. The network topology remains unchanged, allowing the assessment of the existing transmission infrastructure's ability to integrate higher shares of variable renewable energy. The scenario aims to quantify the impact of increased renewable penetration on dispatch patterns, transmission flows, curtailment levels, and operating costs without structural reinforcement of the network.

- **Scenario 3 – Partial Electrification and Hydrogen Blending (E25-BLEND)**

  The third scenario introduces moderate sector coupling, with 25% of thermal demand electrified, shifting part of the heating load from the natural gas network to the electricity system. In parallel, hydrogen is blended into the gas network at a concentration of 15%, reducing the carbon intensity of the remaining gaseous fuel. The gas mixture is treated as pre-mixed, and this assumption is considered valid since hydrogen is injected at an upstream node of the network, allowing perfect mixing before distribution. Consequently, blending is modeled by appropriately modifying the thermophysical properties of the gas mixture. The selected hydrogen blending level is consistent with the upper bounds currently considered in existing European regulatory frameworks for gas transmission systems [16]. This configuration enables evaluation of the combined effects of electrification and hydrogen blending on system operation, including changes in electricity demand, gas network utilization, and the resulting impacts on emissions and operating costs. The electrolyzer, which has a fixed conversion efficiency of 50.5 kWh/kg [17], has been sized to 700 MW to ensure demand coverage.

- **Scenario 4 – High Electrification with Hydrogen for Residual Demand (E75-H_2)**

This scenario represents a more advanced decarbonization pathway characterized by large-scale electrification, with 75% of thermal demand supplied through electricity. The remaining non-electrified thermal demand is met through hydrogen supplied via the existing gas infrastructure, which is assumed to be fully repurposed for hydrogen transport. To support the higher electricity demand associated with both electrification and hydrogen production, renewable generation capacity is further expanded based on the projected installations reported in [15]. This results in an additional 2.89 GW of photovoltaic capacity and 1.98 GW of wind capacity compared to the previous scenario. In addition, 4.0 GWh of battery storage are introduced to provide system flexibility, in line with the development plans outlined in [15]. Electrolyzer capacity is also significantly increased, reaching 4.0 GW, to supply hydrogen for the residual thermal demand.

- **Scenario 5 – Fully Decarbonized Energy System (NET100)**

  The final scenario represents a fully decarbonized regional energy system in which fossil fuels are completely phased out. All energy demand is supplied through renewable electricity and green hydrogen. In this scenario, capacity and transmission constraints are relaxed to ensure the feasibility of the optimization problem under extreme decarbonization conditions. Unlike the previous scenarios, a fully renewable configuration does not admit a feasible solution under current network limits, due to the substantial increase in electricity flows induced by deep electrification and sector coupling. The resulting overloads should therefore be interpreted not as physically admissible operating conditions, but as indicators of the extent and location of the transmission reinforcements required to enable full system decarbonization. Renewable generation and energy storage capacities are therefore treated as decision variables within the optimization process. The resulting configuration requires a substantial expansion of renewable infrastructure, including 9.29 GW of additional photovoltaic capacity and 12.15 GW of additional wind capacity, together with 63 GWh of battery storage. These values highlight the scale of infrastructure deployment required to achieve a fully decarbonized energy system and emphasize the challenges associated with reaching a 100% renewable regional energy supply.

To compare the economic performance of the analyzed scenarios, three complementary cost indicators are evaluated: the Levelized Cost of Final Energy (LCFE), the Levelized Cost of Electricity (LCOE$_{el}$), and the Levelized Cost of Thermal Energy (LCOE$_{th}$), all in €/MWh.

LCFE represents the total system cost normalized over the total final demand (electrical and thermal). It captures the overall economic performance of the integrated energy system and can be represented as in Eq.(9):

$$LCFE = \frac{\sum_{i\in\mathcal{T}}(CAPEX_i \cdot A_i + O\&M_i) + \sum_{t\in T}(P^{dis}_{el,t}\, c^{el}_t + P^{dis}_{gas,t}\, c^{gas}_t)}{E_{el} + E_{th}} \tag{9}$$

where $\mathcal{T}$ is the set of system technologies, $CAPEX_i$ represents capital expenditures annualized through the annuity factor A_i, $O\&M_i$ denotes operation and maintenance costs, $P^{dis}_{el,t}$ is imported electricity at time t, c^{el}_t is the electricity price, $P^{dis}_{gas,t}$ is natural gas consumption, and c^{gas}_t is the natural gas price, while E_{el} and E_{th} represent the total electricity and thermal demand served by the system. Cost of electricity and gas with respectively hourly and daily time steps are retrieved from [18], and a ± 15% is applied for the sensitivity analysis.

To better distinguish the cost structure of the two energy sectors, electricity and thermal costs are further evaluated separately through sectoral levelized cost indicators. The levelized cost of electricity is calculated as:

$$LCOE_{el} = \frac{\sum_{i\in\mathcal{T}_{el}} \alpha^{el}_i (CAPEX_i \cdot A_i + O\&M_i) + \sum_{t\in T} \alpha^{el}_t (P^{dis}_{el,t}\, c^{el}_t + P^{dis}_{gas,t}\, c^{gas}_t)}{E_{el}} \tag{10}$$

Similarly, the levelized cost of thermal energy is defined as:

$$LCOE_{th} = \frac{\sum_{i\in\mathcal{T}_{th}} \alpha^{th}_i (CAPEX_i \cdot A_i + O\&M_i) + \sum_{t\in T} \alpha^{th}_t (P^{dis}_{el,t}\, c^{el}_t + P^{dis}_{gas,t}\, c^{gas}_t)}{E_{th}} \tag{11}$$

Where α^{el} and α^{th} represent the fraction of shared resources allocated to electricity and thermal sectors in scenarios involving sector coupling (such as renewable generation and electricity imports). Since these resources simultaneously contribute to both sectors, their costs are apportioned proportionally to the respective energy use of each sector.

Capital expenditures are annualized using a standard annuity formulation:

$$A_i = \frac{DR(1+DR)^{LT_i}}{(1+DR)^{LT_i} - 1} \tag{12}$$

where DR is the discount rate, assumed at 5%, and LT_i is the lifetime of technology i. Technology-specific life-

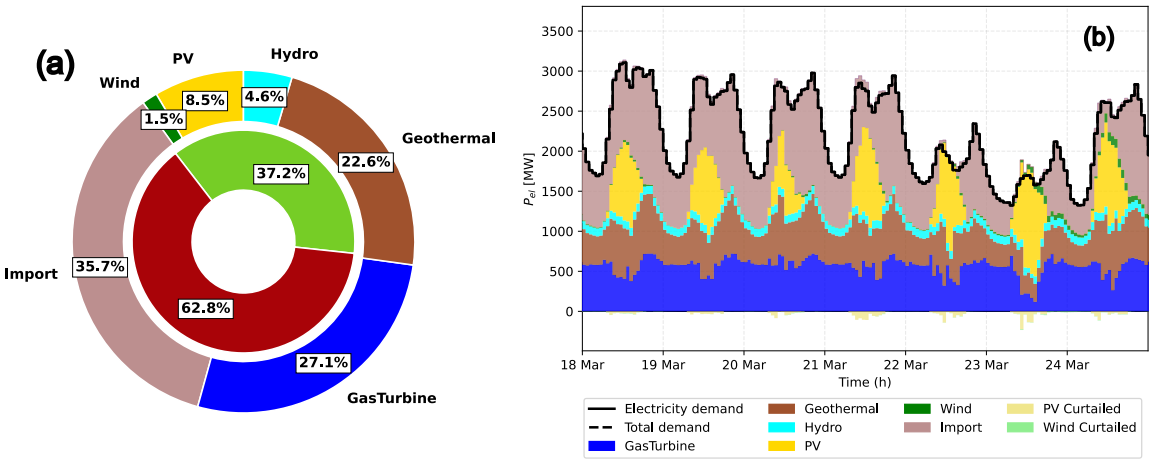

Figure 3. *Pie chart of annual demand coverage (a) and hourly energy balances for a spring week (b).*

times and economic parameters used are reported in Table 1, alongside the sensitivity range for the parameters for which they are employed.

Table 1. *Economic parameters used for the simulation.*

Technology	CAPEX (l-m-h)	OPEX	Lifetime	Ref
PV	680-800-920 €/kW	2%	25	[19]
Wind	850-1000-1150 €/kW	3%	25	[20]
Electrolyzer	200-1200-1400 €/kW	5%	15	[21]
Battery	150-250-350 €/kWh	2.5%	20	[22]
Tank	340-400-460 €/kg	2%	20	[23]

3. Results and discussion

3.1. Energy System Operation and Dispatch Dynamics

In the reference scenario, representative of the current energy configuration of the Tuscany region, thermal demand is entirely supplied by imported natural gas. Electricity demand, instead, is partially met by domestic renewable generation, which accounts for 37.2% of the annual mix, as reported in Figure 3a. The renewable contribution is primarily driven by geothermal energy (22.6%), followed by photovoltaic (8.5%), hydroelectric (4.6%), and wind power (1.5%). Nevertheless, electricity imports (35.7%) and gas turbines (27.1%) remain structurally significant components of the system, confirming a persistent dependence on external supply and thermoelectric generation. Overall, the reference scenario reproduces realistic system-level indicators (such as electricity imports, renewable penetration, gas consumption, and emission levels) supporting the credibility of the adopted synthetic representation of the regional energy system. The weekly dispatch profile for a representative spring week is reported in Figure 3b. It highlights a stable base-load provided by geothermal, gas turbines, and hydroelectric. Photovoltaic generation introduces a clear daytime modulation, reducing the net residual demand during daylight hours. However, wind production remains marginal throughout the week, due to the low capacity installed. As a result, imports continue to play a fundamental role in ensuring adequacy, particularly outside peak solar production periods.

The proposed decarbonization pathways are evaluated from an energetic perspective by analyzing the electricity balances over a representative week in March. Figure 4 presents the dispatch composition for the five scenarios, highlighting the progressive structural transformation of the electricity system. The transition to the RES+ scenario leads to a significant expansion of variable renewable energy, primarily driven by the deployment of wind capacity. This structural shift substantially reduces the contribution of fossil-based generation and lowers the reliance on electricity imports during periods of high renewable output. However, periods of surplus renewable generation become more frequent, potentially leading to curtailment when flexibility options are limited. In the E25–Blend scenario, electricity demand slightly increases due to the combined effects of partial electrification (25%) and the additional consumption associated with hydrogen production via electrolysis. The electrolyzer introduces a new and potentially flexible demand component capable of absorbing excess renewable generation and partially mitigating curtailment. The E75–H_2 scenario represents a more advanced stage of sector coupling. Renewable capacity is further expanded to sustain both the large-scale electrification of thermal demand and the production of hydrogen required to supply the remaining non-electrified energy uses. While this configuration allows a very high renewable penetration, it also amplifies variability in the resid-

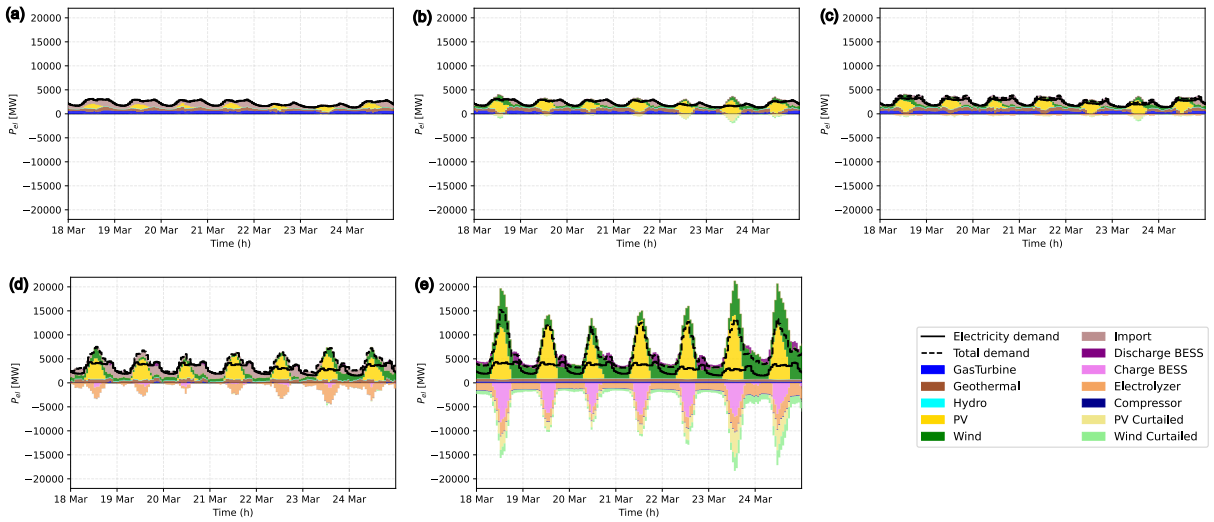

Figure 4. *Hourly energy balances for a spring week for the five scenarios: REF (a), RES+ (b), E25-Blend (c), E75-H_2 (d), NET100 (e).*

ual load. Consequently, during nighttime hours or prolonged low-wind periods, electricity imports remain an important balancing resource despite the substantial increase in renewable generation. Finally, the NET100 scenario illustrates the operational conditions required to achieve a fully decarbonized energy system. In this configuration, fossil generation and import are completely eliminated, and all energy demand must be satisfied through renewable electricity and hydrogen production. As a result, renewable electricity and storage capacity increase significantly to sustain periods of lower production.

Figure 5 compares the annual electricity balances across scenarios, reporting both absolute energy volumes (TWh) and normalized shares (%). The results highlight how changes in generation capacity and demand composition reshape the system's supply mix and carbon intensity. Relative to the reference case (REF), the increased RES (RES+) scenario shows a clear reduction in system carbon intensity driven by renewable expansion. The renewable share rises from 37.2% to 68.3%, mainly due to the deployment of wind and solar capacity. This shift significantly reduces reliance on imported electricity and gas-fired generation. In the E25-Blend scenario, electricity demand increases as a consequence of partial electrification and the introduction of electrolysis for hydrogen production. Since renewable capacity remains unchanged relative to the previous case, the renewable share decreases to 60.3%. At the same time, renewable curtailment declines from 1.57 TWh to 0.90 TWh, as electrolysis provides an additional flexible demand that absorbs 1.83 TWh of electricity and improves renewable utilization. The E75-H_2 scenario further transforms the system. Renewable generation expands significantly, while total electricity demand increases sharply due to large-scale hydrogen production. Although the renewable share stabilizes at around 63%, the system operates at a much higher absolute level of decarbonization due to the thermal sector. Curtailment decreases to 0.53 TWh, largely because electrolyzers consume 9.27 TWh, approximately half of the electricity demand in the reference scenario. Finally, the NET100 configuration represents a fully decarbonized system in which fossil-based generation and electricity imports are completely eliminated. Electricity supply is entirely provided by renewable sources, supported by battery storage and hydrogen-fueled gas turbines for balancing. Achieving this configuration requires a substantial expansion of renewable capacity to meet both direct electricity demand and the additional demand associated with hydrogen production and storage. In this scenario, electricity consumption by electrolyzers and batteries reaches 15.5 TWh and 12.1 TWh, respectively, while renewable curtailment increases significantly to 15.0 TWh due to the large surplus generation required to guarantee full decarbonization.

The implications of the analyzed scenarios on transmission infrastructure can be further assessed by examining the loading of the most stressed power lines. Figure 6 reports the maximum (bars) and average (markers) line loading across the most loaded transmission corridors for each scenario. In the reference and RES+ configurations, most lines operate within acceptable loading ranges, although the increase in renewable penetration already leads to higher peak utilization in some corridors due to spatial mismatches between renewable generation and demand. The E25–Blend and E75–H_2 scenarios further increase network stress as electrification and hydrogen production significantly raise electricity demand and modify flow patterns across the grid. In these configurations, several lines approach their nominal capacity during peak periods, indicating the growing importance of transmission infrastructure in supporting sector coupling and renewable integration. The most critical situation emerges in the NET100 scenario, where the complete electrification of energy services and the large-scale deployment of renewable generation lead to substantially higher power transfers across the network. Several lines experience very high maximum loading levels, with some exceeding 250–300% of their nominal capacity, while average loading also increases significantly. These results indicate that achieving full

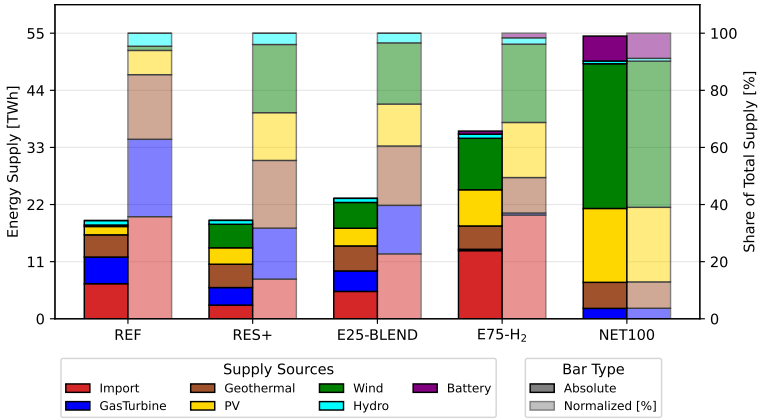

Figure 5. *Comparison of annual energy supply across decarbonization scenarios in absolute terms (TWh) and normalized shares (%).*

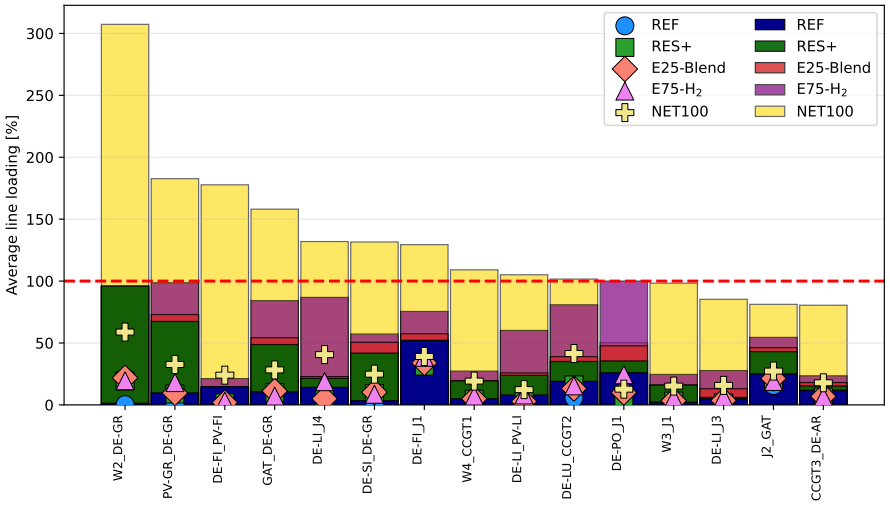

Figure 6. *Maximum (bars) and average (markers) transmission line loading for the most stressed lines across the analyzed scenarios.*

system decarbonization would require substantial reinforcement of the transmission network to accommodate increased electricity flows and stronger spatial coupling between renewable generation sites and demand centers. In contrast, the existing infrastructure is sufficient to handle the operating conditions in the other scenarios.

3.2. Techno-Economic and Environmental Performance

The scenarios are further compared from an economic and environmental point of view. The economic indicators used are the LCFE, LCOE_{el}, and LCOE_{th} described in Section 2.2. Environmental performance is evaluated through annual CO_2 emissions, estimated using carbon intensity factors derived from Electricity Maps for imported electricity and standard emission factors for natural gas [24]. Figure 7a reports LCFE, LCOE_{el}, and LCOE_{th} across the five scenarios, together with their sensitivity ranges. The indicators are decomposed into operational expenditures, fuel and electricity purchase costs, and capital investments associated with new renewable capacity, energy storage, and hydrogen infrastructure. In the reference scenario, system costs are mainly driven by variable expenditures related to natural gas and electricity imports. The LCFE amounts to 53.02 €/MWh, with a sensitivity range between 45.38 and 60.65 €/MWh. The electricity sector exhibits higher costs than the thermal sector: LCOE_{el} reaches 70.15 €/MWh (60.35-79.95 €/MWh), while LCOE_{th} equals 39.60 €/MWh (33.67-45.54 €/MWh), entirely determined by natural gas purchase. Transitioning to the RES+ scenario, the cost structure shifts. Expenditures associated with electricity imports and gas dispatch decline, while capital investments in wind and photovoltaic capacity become contributors. This substitution of fuel-based variable costs with renewable CAPEX improves cost stability and reduces exposure to fuel price volatility. As a result, LCFE decreases to 46.88 €/MWh (40.16-53.59 €/MWh). Since the thermal sector remains entirely dependent on natural gas supply, LCOE_{th} is unaffected. The reduction in LCFE is therefore driven by a decrease in LCOE_{el} to 56.23 €/MWh (48.52-63.94 €/MWh). The E25-Blend scenario introduces sector coupling through partial electrification and hydrogen blending. Additional investments in electrolyzers and hydrogen storage increase capital expenditures, raising LCFE to 52.52 €/MWh (43.01-63.14 €/MWh). In this configuration, sector-coupling related components start to appear within the thermal cost structure. Consequently,

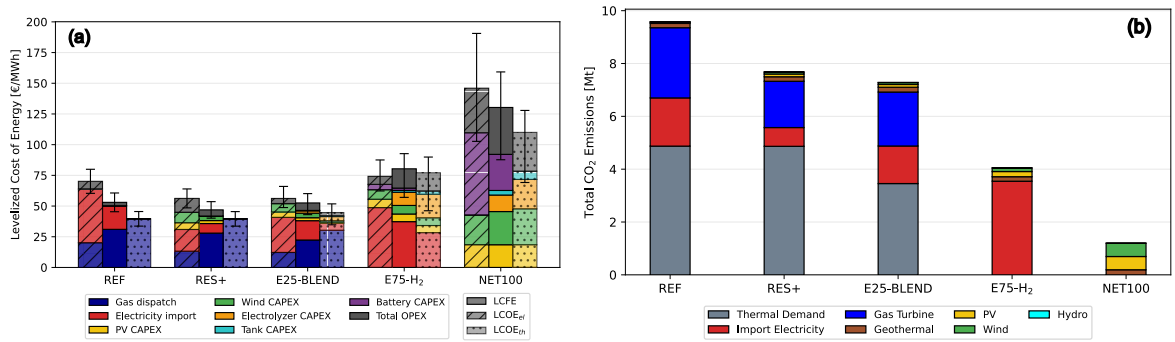

Figure 7. *Comparison of economic (a) and environmental (b) performance of decarbonization scenarios.*

$LCOE_{th}$ increases to 44.72 €/MWh, showing a wider sensitivity range due to uncertainty associated with electrolyzer investment costs (34.72-51.78 €/MWh). By contrast, $LCOE_{el}$ remains almost unchanged, as the additional electricity consumption is primarily linked to hydrogen production rather than direct electricity demand. The E75-H_2 represents a deeper structural transformation of the energy system. Extensive electrification and large-scale hydrogen production require substantial investments in renewable generation and hydrogen infrastructure. As a result, LCFE rises to 80.33 €/MWh (57.07-92.02 €/MWh). Both sectoral indicators increase: $LCOE_{el}$ reaches 74.20 €/MWh (62.28-87.54 €/MWh), while $LCOE_{th}$ increases to 77.16 €/MWh (46.18-89.90 €/MWh), again showing higher variability due to the sensitivity of electrolyzer-related investments. Finally, the NET100 scenario represents the most capital-intensive configuration. Achieving full decarbonization requires very large investments in renewable generation, battery storage, and hydrogen infrastructure. Consequently, LCFE increases substantially to 130.28 €/MWh, with a wide sensitivity range between 87.71 and 159.24 €/MWh. Both sectoral indicators increase significantly due to the complete restructuring of the energy system: $LCOE_{el}$ reaches 146.00 €/MWh (102.68–190.59 €/MWh), while $LCOE_{th}$ rises to 110.01 €/MWh (69.18–127.88 €/MWh). The wider uncertainty ranges reflect the strong dependence of this scenario on capital-intensive technologies such as large-scale renewable deployment, hydrogen production, and energy storage.

The economic implications of the proposed decarbonization pathways can be more rigorously assessed by linking incremental system costs to the corresponding emission reductions. As shown in Figure 7b, the transition from the REF configuration to the alternative pathways leads to a progressive reduction in annual CO_2 emissions. In the reference scenario, total emissions amount to 9.58 Mt_{CO_2}. The largest contribution originates from natural gas consumption for thermal demand. In the electricity sector, emissions are mainly associated with natural gas combustion in gas turbines used to balance demand and complement renewable generation. The transition to the RES+ scenario produces a substantial emission reduction, with total emissions declining from 9.58 Mt_{CO_2} to 7.68 Mt_{CO_2}. This decrease is primarily driven by the expansion of wind and photovoltaic capacity, which reduces the reliance on both imported electricity and gas-fired generation. In contrast, the E25-Blend scenario yields only limited additional emission reductions, with emissions decreasing marginally to 7.29 Mt_{CO_2}. The reduction in direct natural gas consumption due to partial electrification is partly offset by increased electricity demand and continued reliance on imports, as renewable capacity remains unchanged compared to the previous scenario. Furthermore, hydrogen blending at 15% provides only modest emission savings. These results indicate that electrification alone does not guarantee substantial emission reductions unless accompanied by a parallel expansion of renewable generation, and that moderate hydrogen blending mainly acts as a transitional measure with limited impact on total emissions. The E75-H_2 configuration achieves a much deeper decarbonization, with emissions declining to 4.05 Mt_{CO_2}. In this configuration, natural gas supply for thermal demand is entirely eliminated and replaced by electrification and hydrogen. As a consequence, the remaining emissions are largely associated with the electricity sector, particularly with imported electricity used to meet the increased demand resulting from electrification and hydrogen production. Finally, the NET100 scenario achieves near-complete decarbonization of the system. In this configuration, both fossil fuel consumption and electricity imports are eliminated, and the remaining 1.20 Mt_{CO_2} are associated exclusively with the life-cycle emissions of renewable energy technologies.

Overall, the analysis highlights a clear decarbonization pathway. Initial renewable deployment provides substantial emission reductions by displacing fossil-based electricity generation. Deeper decarbonization requires the progressive electrification of energy services and the integration of hydrogen as an energy carrier, supported by a significant expansion of renewable generation capacity. These results underline the importance of coordinated renewable deployment and sector coupling strategies in achieving deep emission reductions in regional energy systems.

A synthetic comparison of the main technical, environmental, and economic indicators across scenarios is reported in Table 2.

Table 2. *Comparison of key performance indicators across scenarios.*

Indicator	REF	RES+	E25-Blend	E75-H_2	NET100
PV Capacity [GW]	1.47	3.29	3.29	6.18	15.46
Wind Capacity [GW]	0.15	2.39	2.39	4.37	16.52
Electrolyzer Capacity [GW]	-	-	0.7	4.0	5.0
Battery Capacity [GWh]	-	-	-	4.0	63.0
RES share [%]	37.2	68.3	60.3	63.0	100.0
LCFE (l-m-h) [€/MWh]	45.4-53.0-60.7	40.2-46.9-53.6	43.0-52.5-60.1	57.1-80.3-92.7	87.7-130.3-159.2
$LCOE_{el}$ (l-m-h) [€/MWh]	60.4-70.2-79.9	48.5-56.2-63.9	48.8-56.2-66.0	62.3-74.2-87.5	102.7-146.0-190.6
$LCOE_{th}$ (l-m-h) [€/MWh]	33.7-39.6-45.5	33.7-39.6-45.5	34.7-44.7-51.8	46.2-77.2-89.9	69.2-110.0-127.9
Total emissions [Mt_{CO_2}]	9.58	7.68	7.29	4.05	1.20

4. Conclusions

This study investigated the feasibility and implications of alternative decarbonization pathways for a regional multi-energy system through a spatially explicit optimization framework integrating electricity, natural gas, and hydrogen infrastructures. The proposed model explicitly represents nodal energy balances, transmission constraints, and sector-coupling technologies, enabling a consistent assessment of energy flows, infrastructure utilization, and system costs under progressively more ambitious decarbonization scenarios.

The results highlight that renewable expansion represents the most cost-effective initial decarbonization strategy. Increasing wind and photovoltaic capacity significantly reduces both system costs and emissions by lowering dependence on imported electricity and fossil fuel generation. However, partial electrification combined with moderate hydrogen blending (E25-Blend) yields only limited additional emission reductions when renewable capacity remains unchanged, demonstrating that electrification alone is insufficient without parallel renewable deployment. Deeper decarbonization pathways characterized by extensive electrification and hydrogen integration substantially reduce system emissions but require large investments in renewable generation and hydrogen infrastructure. In particular, the E75–H_2 scenario achieves major emission reductions but significantly increases the levelized cost of final energy due to the capital-intensive nature of electrolyzers, renewable capacity expansion, and storage technologies. The fully decarbonized NET100 scenario highlights the scale of infrastructure transformation required to eliminate fossil fuels completely. Achieving this configuration requires massive deployment of renewable capacity and energy storage. The results also show that current transmission infrastructure would become a critical bottleneck under such conditions, as several lines experience substantial overloading in the absence of grid reinforcement.

Overall, the analysis reveals a clear decarbonization trajectory: early renewable deployment provides substantial emission reductions at relatively low cost, whereas deeper decarbonization requires increasing reliance on sector coupling, hydrogen integration, and large-scale infrastructure investments. These findings underline the importance of coordinated planning of renewable deployment, transmission expansion, and hydrogen infrastructure development to ensure both the economic feasibility and operational reliability of deeply decarbonized regional energy systems. Notwithstanding these insights, some limitations of the proposed modeling framework should be acknowledged. The analysis is based on a deterministic setup and has not been validated against real operational data, which may affect the representativeness of the results under actual system conditions. Furthermore, several modeling assumptions, such as simplified representations of hydrogen blending and infrastructure operation, may influence the quantitative outcomes and should be refined in future work.

Nomenclature

Letter symbols

A	Annuity factor, -	$LCOE_{th}$	Levelized cost of thermal energy, €/MWh
C	Cost, €	LT	Lifetime, yr
Cap	Line capacity, MW	$\dot{m}$	Mass flow rate, kg/s
$CAPEX$	Capital expenditure, €	$O\&M$	Operation and maintenance, €
c	Specific cost, €/MWh	P	Power, MW
$dist$	Euclidean distance, km	p	Pressure, Pa
DR	Discount rate, -	R_{gas}	Specific gas constant, kJ/(kg K)
E	Energy, MWh	r	Line resistance, MW^{-1}
f	Darcy friction factor, -	T	Temperature, K
$LCFE$	Levelized cost of final energy, €/MWh	x	Line reactance, MW^{-1}
$LCOE_{el}$	Levelized cost of electricity, €/MWh	Z	Compressibility factor, -

Greek symbols

α	Share
θ	Voltage Angle

Subscripts and superscripts

$curt$	Curtailment	$grid$	Import	$O\&M$	Operation and maintenance
dem	Demand	in	Inflow	out	Outflow
dis	Dispatch	$loss$	Loss	th	Thermal
el	Electricity	max	Maximum	t	Timestep
gas	Gas	min	Minimum	v	Vector

References

[1] van der Zwaan B, Fattahi A, Dalla Longa F, Dekker M, van Vuuren D, Pietzcker R, et al. Electricity- and hydrogen-driven energy system sector-coupling in net-zero CO2 emission pathways. Nat Commun. 2025;16(1):1368.

[2] IRENA Coalition for Action. Sector coupling: A key concept for accelerating the energy transformation. International Renewable Energy Agency, Abu Dhabi; 2022.

[3] Kountouris I, Bramstoft R, Madsen T, Gea-Bermúdez J, Münster M, Keles D. A unified European hydrogen infrastructure planning to support the rapid scale-up of hydrogen production. Nat Commun. 2024;15(1):5517.

[4] Raycheva E, Akbari B, Garrison J, Hug G, Schaffner C, Sansavini G. The value of power-to-gas-to-power in Switzerland 's electricity system planning. Energy. 2025;330:136451.

[5] Mancò G, Tesio U, Guelpa E, Verda V. A review on multi energy systems modelling and optimization. Appl Therm Eng. 2024;236:121871.

[6] Prina MG, Manzolini G, Moser D, Nastasi B, Sparber W. Classification and challenges of bottom-up energy system models - A review. Renewable Sustainable Energy Rev. 2020;129:109917.

[7] Neumann F, Hagenmeyer V, Brown T. Assessments of linear power flow and transmission loss approximations in coordinated capacity expansion problems. Appl Energy. 2022;314:118859.

[8] Guzzo G, Francesconi M, Carcasci C. Smart management of pressure regulating stations to maximize hydrogen injection in a gas distribution network. Int J Hydrogen Energy. 2024;69:626-34.

[9] Snam. Gas network and transport infrastructure;. Available at https://www.snam.it/it/i-nostri-business/trasporto/informazioni-commerciali/rete-gas-e-infrastrutture-trasporto-gas.html [accessed 23.03.2026].

[10] OpenInfraMap. Open Infrastructure Map;. Available at https://:www.openinframap.org/ [accessed 23.03.2026].

[11] RSE. Integrated Atlas for the Italian National Energy System;. Available at https://atlanteintegrato.rse-web.it/ [accessed 23.03.2026].

[12] CEI. CEI 11-60: Thermal capacity of outdoor overhead power lines with a voltage greater than 100 kV;. Available at https://mycatalogo.ceinorme.it/cei/item/000006507?sso=y [accessed 23.03.2026].

[13] European Commission, JRC. Photovoltaic Geographical Information System;. Available at https://re.jrc.ec.europa.eu/pvg_tools/en/ [accessed 23.03.2026].

[14] MASE - Italian Ministry of the Environment and Energy Security. Provincial Natural Gas Consumption;. Available at https://sisen.mase.gov.it/dgsaie/consumi-provinciali-gas-naturale [accessed 23.03.2026].

[15] Terna. Econnextion: Map of Renewable Energy and Storage Connections – Connection Requests by Province;. Available at https://dati.terna.it/econnextion [accessed 23.03.2026].

[16] European Hydrogen Observatory. The European hydrogen policy landscape - January 2026;. Available at https://observatory.clean-hydrogen.europa.eu/tools-reports/observatory-reports [accessed 24.03.2026].

[17] Calabrese M, Ademollo A, Carcasci C. Designing off-grid hybrid renewable energy systems under uncertainty: A two-stage stochastic programming approach. Renewable Energy. 2026;256.

[18] GME. Energy Market Results;. Available at https://www.mercatoelettrico.org/it-it/Home/Esiti/ [accessed 23.03.2026].

[19] NREL. Annual Technology Baseline: Utility-Scale PV; 2024. Available at https://atb.nrel.gov/electricity/2024b/utility-scale_pv [accessed 23.03.2026].

[20] NREL. Annual Technology Baseline: Land-Based Wind; 2024. Available at https://atb.nrel.gov/electricity/2024b/land-based_wind [accessed 23.03.2026].

[21] IRENA. Making the breakthrough: Green hydrogen policies and technology costs. International Renewable Energy Agency, Abu Dhabi; 2021.

[22] Cole W, Ramasamy V, Turan M. Cost Projections for UtilityScale Battery Storage: 2025 Update;. Available at https://www.nrel.gov/docs/fy25osti/93281.pdf [accessed 23.03.2026].

[23] Ademollo A, Calabrese M, Carcasci C, Joshi I, Vaccaro M. Comparative techno-economic assessment of stationary hydrogen storage technologies. Int J Hydrogen Energy. 2026;199.

[24] Electricity Maps. Emission Factors;. Available at https://app.electricitymaps.com/dashboard [accessed 24.03.2026].